Intermolecular Coupling Related Electrical Transport Transition in Vanadyl–Phthalocyanine (VOPc) Molecular Bilayers

ARTICLE *in* THE JOURNAL OF PHYSICAL CHEMISTRY C · AUGUST 2012

Impact Factor: 4.77 · DOI: 10.1021/jp304103g

3 AUTHORS, INCLUDING:

Weiguang Xie

Jinan University (Guangzhou, China)

55 PUBLICATIONS **346** CITATIONS

THE JOURNAL OF PHYSICAL CHEMISTRY C

Article

pubs.acs.org/JPCC

Intermolecular Coupling Related Electrical Transport Transition in Vanadyl-Phthalocyanine (VOPc) Molecular Bilayers

Weiguang Xie,[†,‡] Xiaomu Wang,[‡] and Jianbin Xu*[,‡]

[†]Siyuan Laboratory, Department of Physics, Jinan University, Guangzhou, Guangdong, China

[‡]Department of Electronic Engineering, and Materials Science and Technology Research Center, The Chinese University of Hong Kong, Shatin, Hong Kong

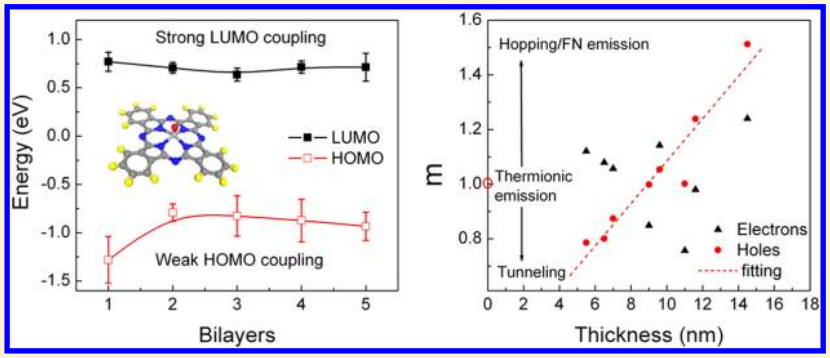

ABSTRACT: We demonstrate the correlation between intermolecular coupling and electrical transport in VOPc molecular bilayers. The intermolecular electrical interaction is estimated by scanning tunneling spectroscopy. We find that the stronger coupling of LUMO−LUMO between VOPc molecular bilayers leads to thickness-independent LUMO positions and contact-dominating electron transport. On the other hand, intermolecular coupling of HOMO−HOMO is less; therefore, the measured HOMO positions are thickness-dependent, and transition from thermionic emission to Frenkel-Poole transport and to field emission can be observed with increasing thickness and applied bias. The findings show that the intermolecular coupling and electrical transport behavior can be revealed in situ at the same time, which is helpful in understanding the fundamental transport mechanism in organic semiconductors.

INTRODUCTION

Charge transport is an important issue in organic electronics. In the field of organic semiconductors, there have been many experiments on the transport of single molecule,[1,2] thin film, and single crystal.[3−5] However, the transport mechanism is still controversial,[6−8] because the transport behavior strongly depends on the intermolecular coupling and reorganization of molecules, which are affected by thermal effects, charging, and stacking.[2,9,10] Scanning tunneling microscopy (STM) has been widely used to study the electrical transport in organic semiconductors.[1,11,12] STM has high spatial resolution to resolve the geometric stacking of the molecules. In addition, the tip of the STM can be applied as one of the electrodes to study the electrical transport of a single molecule.[11] The STM tunneling process in organic molecules is mediated by the molecular orbitals.[13,14] In a previous study on CuPc molecules on a thin oxide film by STM, Wu et al. showed that the shifting of the energy levels of the molecule is controlled by the ratio between the tunneling rates of tip−sample and that through the oxide thin film.[2] Recently, Gopakumar[15,16] and other researchers[17] have reported that the shifting of the HOMO position with the variation of the tip−sample distance is different from that of the LUMO position, which is the result of the difference between the coupling of the LUMO−substrate and the coupling of the HOMO−substrate. The findings imply that, by measuring the movement of HOMO and LUMO behaviors with the variation of the tip−sample distance, the electrical coupling intensity can be estimated separately.

In recent years, length-dependent electrical transport in molecular wires has been reported by current−voltage (I−V) measurements using scanning probe microscopy.[18] The exponential length dependent resistance is verified clearly. It is also observed that the behavior of the transport is described by different transport models depending on the molecular length[19] and molecular conformation.[20] Based on the methods developed in these works, it is also possible to reveal the layer-dependent transport mechanism by I−V measurements and energy level measurements in molecular thin films; however, there are few reports on the change of the electrical transport process from a single layer to a thin film.[21] In this study, by using a VOPc molecular thin film as a model system, we show the effect of intermolecular coupling on the change of energy level at the interface between the VOPc thin film and the

Received: April 28, 2012
Revised: July 15, 2012
Published: August 2, 2012

   dx.doi.org/10.1021/jp304103g | J. Phys. Chem. C 2012, 116, 17580−17585

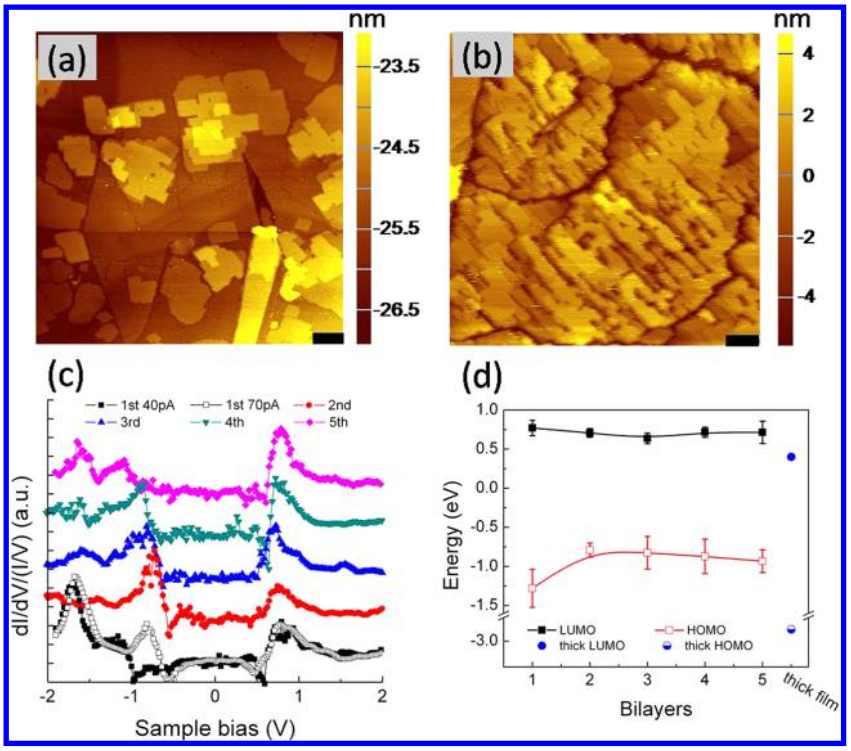

Figure 1. Panels a and b are STM topography images of a thin (the scale bar is 50 nm) and a thick (the scale bar is 100 nm) VOPc thin film on HOPG surface, respectively. (c) Typical normalized scanning tunneling spectroscopy from the 1st to the 5th bilayer. The sample bias before STS measurements of the 2nd to 5th bilayer is +1.5 V and the current set point is 40 pA. Two current set point values (40 and 70 pA) are used for the 1st bilayer, which means that the STS are measured at different tip−sample distance. (d) The measured HOMO and LUMO positions from the scanning tunneling spectroscopy.

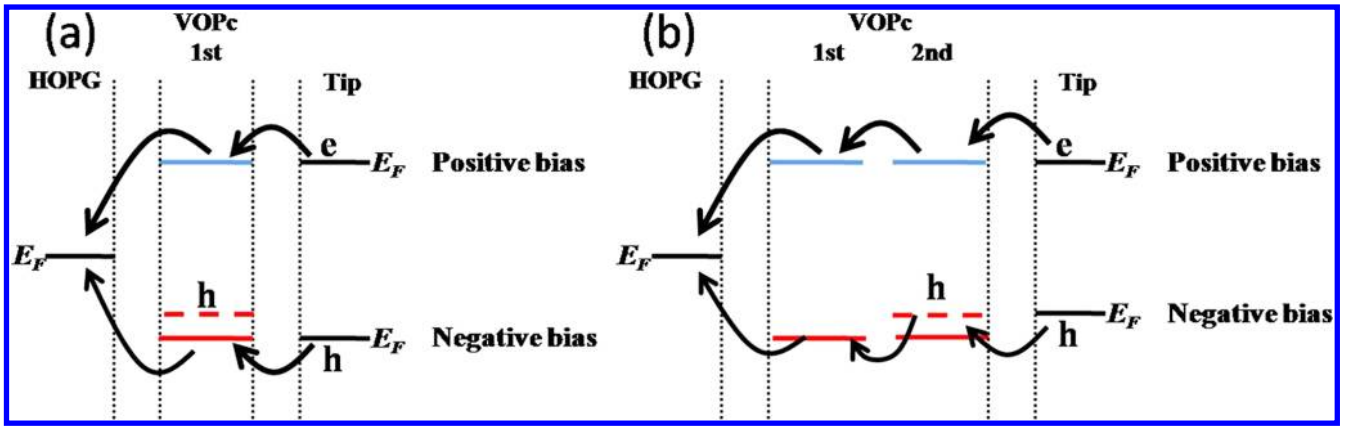

Figure 2. Schematic energy diagram of the tunneling processes in VOPc bilayers. (a) Charging of 1st bilayer and (b) transport in thin film with 2 bilayers. Solid lines indicate the intrinsic levels of the molecules and the dash lines indicate the charged levels.

HOPG substrate and reveal the transition of the electrical transport process from a single molecular bilayer to a thin film.

■ EXPERIMENTAL SECTION

VOPc molecules were purchased from Alfa Aesar and purified by three cycles of sublimation. The HOPG substrate was cleaved in air and then immediately transferred into the deposition chamber with a base pressure of 2×10^{-8} mbar. VOPc molecules were deposited onto the HOPG substrate at a rate of 0.5−1.0 nm/min. During the deposition, the HOPG substrate was kept at room temperature. After the VOPc molecules were prepared, the sample was transferred without exposure to air to the analysis chamber equipped with a RHK UHV 300 STM system with a base pressure of 1×10^{-9} mbar. Each scanning tunneling spectroscopy (STS) run was averaged by five repeated measurements. The values of HOMO and LUMO positions of each bilayer were calculated from more than five STS runs measured separately (Figure 1d). The Z−V curves are measured by ramping the sample bias from ±2 to ±50 mV with the feedback enabled. The contact $I-V$ curves were measured by bringing the tip 1 nm forward to the surface as compared to the imaging tunneling position, which ensures the formation of stable tip−sample contact. Although the process generally cause damages to the topmost molecular monolayer (~0.2−0.3 nm), the effect will not lead to a fundamental difference in the thickness range with which we are concerned as discussed in the related section.

dx.doi.org/10.1021/jp304103g | J. Phys. Chem. C 2012, 116, 17580−17585

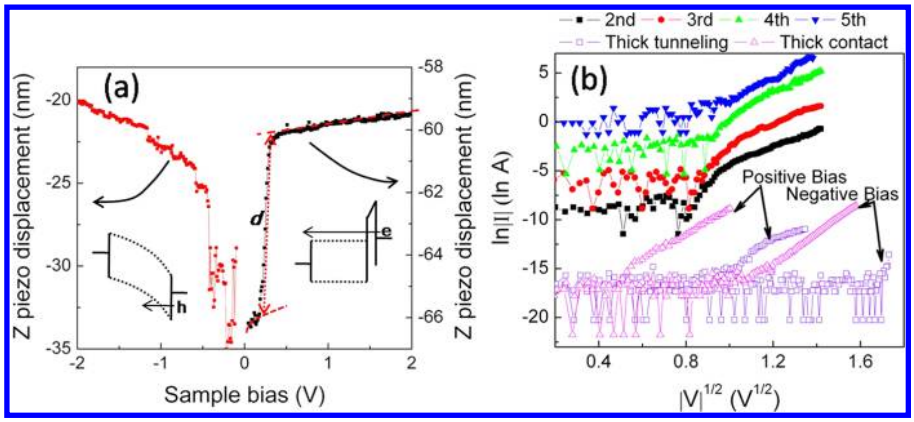

Figure 3. (a) Z−V curves on thick films, the tunneling set point is +1.5 V, 20 pA; the insets at positive side and negative side show the relative band diagram before the abrupt jump of the tip respectively; (b) ln $I \approx |V|^{1/2}$ curves for thin film with different thickness. The second to fifth I−V curves correspond to the parts of STS curves under negative sample bias in Figure 1(c). Curves are offset for easy reading.

RESULTS AND DISCUSSION

Figure 1a,b shows the topography of absorbed VOPc molecules on the HOPG surface. In our former study, we have pointed out that the VOPc molecules adopted cofacial bilayer growth. The VOPc molecules will form a fully covered bilayer on the HOPG surface first, after which islands with multiple molecular bilayers will grow.[22] The molecules in the bilayers are lying down, and the height of each bilayer is 0.7−0.8 nm. Figure 1c shows a set of normalized tunneling spectra measured on the first to the fifth bilayers. The vacuum level of the VOPc molecular thin film aligns with that of the HOPG substrate (work function 4.6 eV).[23] The electron affinity calculated from the first energy level (LUMO) above the Fermi level in Figure 1c is 3.89 eV (4.6 − 0.71 = 3.89 eV), which agrees with that of VOPc molecules absorbed on the Au surface.[24] Besides, the observed average LUMO−HOMO gap of the first bilayer is about 2 eV, which agrees with the band gaps of metal-lophthalocyanines.[15,16,24]

The coupling of LUMO−HOPG and that of HOMO−HOPG are compared by the STS measurement on the first bilayer. The spectra are measured under tunneling current set points of 40 and 70 pA. A higher tunneling current set point means smaller tip−sample distance (Figure 1c). It is clearly shown that the HOMO position moves toward the Fermi level when the tip−sample distance decreases. At the same time, the LUMO position remains unchanged. This observation indicates that VOPc molecules are similar to the d^8 metallophthalocya-nine.[15,16] There are two tunneling processes involved (Figure 2a): (1) tunneling between the tip and the molecular bilayer and (2) tunneling between the molecular bilayer and the substrate (the intermolecular tunneling in the bilayer is not considered as the molecules in the bilayer form much stronger coupling, which ensure that it will not be the limiting factor discussed here). In VOPc molecules, the HOMO is composed of π electrons that are parallel to the substrate, which means the coupling and transfer of holes between the molecules and the substrate are weak.[15,16] Therefore, when the STM tip approaches the surface, the tunneling rate at the tip−molecule side will exceed the rate at the substrate−molecule side, during which the molecule is charged with holes and the HOMO position is moved to the Fermi level (Figure 2a). In contrast, the d_z orbital from the center V atom contributes to the LUMO orbital. As the d_z orbital is normal to the molecular plane, it couples stronger with the substrate.[15,16] Electrons injected from the tip can be transferred from the LUMO to the substrate without delay as the tip−sample distance decreases. Therefore, the LUMO position is pinned when tip−sample distance changed.

The measured LUMO and HOMO positions on the first to the fifth bilayer are shown in Figure 1d. The LUMO positions keep approximately the same around 0.71 eV from the first to the fifth bilayers, indicating that the electron transport is not limited by the interbilayer interaction. At the same time, we observed that the HOMO positions on the second to the fifth bilayer moved to the Fermi level by 0.5−0.4 eV relative to that of the first bilayer. Considering that the coupling of HOMO−HOPG can not lead to the shifting of HOMO under the current tunneling set point (40 pA), we can conclude that the HOMO coupling between molecular bilayers is weaker but the mechanism is similar to that of the HOMO−HOPG. When the sample is negatively biased, for example, holes injection from the tip to the molecules in the second bilayer (Figure 2b), the smaller tunneling rate between the second bilayer and the first bilayer will cause the delay of holes transfer; therefore, the molecules in the second bilayer are charged. The HOMO position of the second bilayer thus shifts to the Fermi level accordingly until the tunneling rates of bilayer/substrate, bilayer/bilayer, and bilayer/tip come to a balance. As the same charging process takes effect, all of the HOMO positions of the third to fifth bilayer move upward to the Fermi level relative to that of the first bilayer.

Besides, we also observed that the shifting value of the HOMO position decreased when the bilayer number increased. For comparison, we measured the tunneling spectra on a thick film shown in Figure 1b. An obvious rectifying effect was observed. When the film thickness increases, the HOMO position will shift away from the Fermi level quickly to about −3 eV, whereas the shifting of the LUMO position is relatively small as compared to that of the HOMO position.

Rectifying behavior in a molecular system can be caused by D-σ-A configuration[25] or contact effect.[26] In this case, there is only one type of molecule weakly adsorbed on the HOPG surface and the bilayer staking is symmetric. In addition, the work function of the tungsten tip is 4.5 eV,[27] close to that of HOPG (4.6 eV); therefore, the rectifying behavior should be caused by other effects. The effect from adsorbates should be excluded because the preparation and measurement procedures are carried out in situ in UHV condition. The slight tilt of molecules can be determined from the observed bilayer height

dx.doi.org/10.1021/jp304103g | J. Phys. Chem. C 2012, 116, 17580−17585

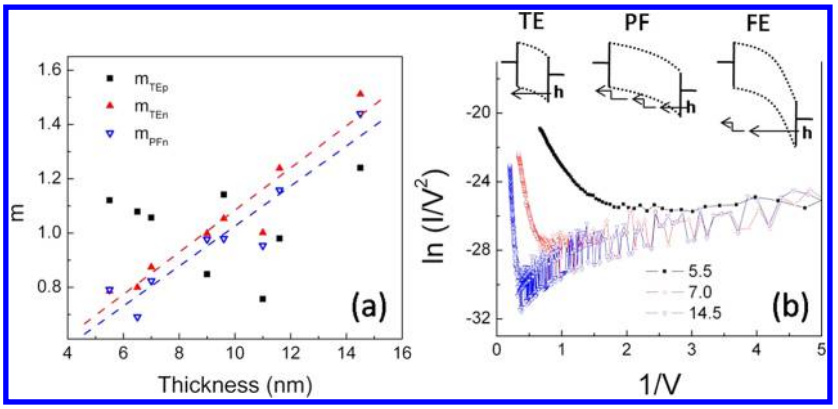

Figure 4. (a) m values extracted using eqs 1 and 2; m_{TEp} and m_{TEn} are the m values extracted by the TE model under positive bias and negative bias respectively; m_{PFn} is the m values extracted by the PF model under negative bias; (b) FN plots at negative bias for film thickness at 5.5, 7.0, and 14.5 nm. The insets show the energy diagram at different thickness and bias when TE, PF, and FN models take effect.

between 0.8 and 0.9 nm in thick film. However, the bilayer height remains between 0.7 and 0.8 nm from the first to the fifth bilayers, which manifests their lying down configuration. Therefore, we consider that the change of orientation may affect the energy level alignment and carrier transport, but should not be the dominating effect here. It has been pointed out experimentally and theoretically that, in organic thin film on a smooth substrate, the charge injection from the tip (no matter tunneling or in contact with surface) is much more efficient than that from the plane substrate, which means that charge injection from the tip is the dominating process.[28] Therefore, we suggest that the rectifying behavior in our case is caused by the difference between molecular coupling of LUMO−LUMO and that of HOMO−HOMO, which have different influences to electrons and holes transfer.

As the coupling of HOMO−HOMO is weaker than that of LUMO−LUMO, we conclude that the transport of holes is slower than that of electrons, and thus hole mobility as well as the conductance from holes is smaller. With the thickness increasing, the hole conductance should greatly decrease accordingly. This is confirmed by measuring the Z−V curves at both positive and negative bias (Figure 3a). Under positive bias, the tip position decreases by ∼0.2 nm/V when the bias is above +0.7 V. This means that electron tunneling between the thin film and the tip is the dominating process (as shown in the inset in Figure 3a). Under negative bias when holes are injected by the tip, the tip decreases by ∼3 nm/V. As normal tunneling gap is 0.7−0.8 nm, the dramatic change of tip position means that the resistance of the thin film is larger than that of the tunneling gap so that most of the bias drops on the film at negative bias. As a result, when measuring the $I-V$ curve of a thicker film under negative bias, a portion of bias would drop at the film itself. The shifting of HOMO position with the number of bilayer increased from 2 to 5 reflects the redistribution of bias on sample as shown in the inset of Figure 3a. Voltage drop on the molecular thin film under STM have been observed theoretically and experimentally.[21,29]

With the thickness increasing, the transport behavior is also changing. Four transport models such as thermionic emission (TE, eq 1), Poole-Frenkel (PF, eq 2) transport, Fowler-Nordheim (FN, eq 3) emission and space-charge-limited current (SCLC, eq 4) are considered.

$$I \propto A^{*}T^{2} \exp\left[mB\sqrt{V} - \frac{q\phi_{B}}{kT}\right] \quad (1)$$

$$\frac{I}{V} \propto \exp\left[mB\sqrt{V} - \frac{q\phi_{B}}{kT}\right] \quad (2)$$

$$\frac{I}{V^{2}} \propto \exp\left[\frac{-4d\sqrt{2m_{e}\phi_{B}^{3}}}{3\hbar q}\left(\frac{1}{V}\right)\right] \quad (3)$$

$$I \propto \frac{9\varepsilon_{r}\varepsilon_{0}\mu V^{2}}{8d^{3}} \quad (4)$$

where A^{*} is the effective Richardson constant, ϕ_{B} is the effective barrier height, m_{e} is the effective mass of electron, and $B = q^{3/2}/kT(4\pi\varepsilon_{r}\varepsilon_{0}d)^{1/2}$. The dielectric constant of VOPc is assumed to be 1.22 as that of TiOPc.[30] The thickness d can be estimated from Z−V curves as shown in Figure 3a.

SCLC model can be ruled out as it does not fit any of the I−V curves here. Figure 3b shows that the $\ln(I) \approx V^{1/2}$ curves under negative sample bias change gradually from nonlinear to linear with bilayer number increases, while the $\ln(I) \approx V^{1/2}$ curves under positive bias remain unchanged (similar to that on the second bilayer in Figure 3b). When the tip is brought into contact with the surface, the $\ln(I) \approx V^{1/2}$ curves (TE model) at both positive and negative bias are linear, and we also find that the $\ln(I/V) \approx V^{1/2}$ curves (PF model) are linear too.

The difference between TE and PF model can be distinguished by the m value. For a typical TE transport model, the m value extracted from eq 1 exactly equals 1. For a typical PF transport model, the m value extracted from eq 2 exactly equals 2. Figure 4a shows the m values calculated from the measured contact $I-V$ curves of difference thickness using eqs 1 and 2, respectively. For the contact $I-V$ curves under negative bias, the values of m_{TEn} increase from 0.78 to 1.5 when the film thickness increases. The values of m_{PFn} are smaller but the tendency is the same. The thickness-dependent m values suggest a correlation between the transport mechanism of hole and the film thickness. When the film thickness decreases, the smaller m_{TEn} values (<1) suggest that the thermal emission process of hole is replaced by the tunneling process gradually. The $\ln(I) \approx V^{1/2}$ will become nonlinear as tunneling process dominates (e.g., the $\ln(I) \approx V^{1/2}$ curves of the fourth bilayer in Figure 3b). When the film grows thicker, the m_{TEn} values is bigger than 1. At the same time, the values of m_{PFn} also increase. The STS measurements (Figure 1d) have demonstrated that the molecules are charged during the hole transport process; therefore, hoping of holes between molecular bilayers

dx.doi.org/10.1021/jp304103g | J. Phys. Chem. C 2012, 116, 17580−17585

is believed to become obvious as the film thickness increases. Although the observed maximum value of m_{PFn} is still smaller than 2, it suggests that the transition from TE dominated transport to PF dominated transport starts as the film thickness increases.

For positive bias, the m_{TEp} values fluctuated between 1.1 and 0.77 (the variation of m_{PFp} values is similar to that of m_{TEp}). When the tip is brought into contact with the surface, it is inevitable to damage the topmost bilayer. As the intrinsic resistance under positive bias is very small, thermionic emission from the tip plays dominating effect. However, as it is hard to control the contact status, the m_{TEp} values become scattered around 1 due to the contact effect.

FN behaviors with a low bias tunneling region, a high bias field emission region and a transition region between them have been reported in molecular wires.[18] However, the authors found no reasonable parameters using TE, PF and SCLC model, and the mechanism of the transition region is still not clearly assigned. From the FN plots in Figure 4b, we find that there is also a transition behavior from low bias to high bias as the film thickness increases. For the area with thickness of 5.5 nm, the FN curve goes smoothly upward as the bias increases and no linear relationship is found. This confirms that tunneling and TE model dominates. The holes tunneled or thermally injected from the tip are less scattered by the thin molecular layers. With thickness increase, we observed a dip in the FN plot as the voltage increases. The FN curves turn upward and a linear relationship can be observed at high bias, showing that field emission occurs. As the thickness increases, the injected holes have to travel a long path before they reach the opposite electrode. Therefore, hopping behavior will become obvious before field emission starts. FN plots observed at positive bias for all thickness observed are similar to that of 5.5 nm in Figure 4b, which agrees with the analysis using TE and PF models. Considering the analysis using the three models, we can conclude that the electron transport in contact condition is thermionic emission, whereas the hole transport experiences a transition from thermionic emission (or tunneling in very thin film) to PF transport and to field emission depending on the thickness and the bias (insets in Figure 4b).

CONCLUSION

We have shown that the difference between intermolecular coupling of LUMO−LUMO and that of HOMO−HOMO in VOPc molecular thin films can be estimated through the tip−sample distance dependent STS measurement. The charge transport mechanism is determined by the coupling difference. Intrinsic VOPc molecular thin film favor electron transport because of stronger LUMO coupling. Hole transport is restricted due to the weak intermolecular HOMO coupling, therefore thickness dependent transport behavior can be observed. Tip−sample distance dependent LUMO/HOMO behavior has been revealed in many systems such as d^8 phthalocyanines/HOPG, naphthalocyanine/HOPG, and SnPc/Ag(111). We can expect that, revealing the geometry of a molecular thin film, intermolecular interaction and transport characteristics using STM in situ can be applicable in the illustration of the transport mechanism of organic thin films.

AUTHOR INFORMATION

Corresponding Author

*E-mail: jbxu@ee.cuhk.edu.hk.

Notes

The authors declare no competing financial interest.

ACKNOWLEDGMENTS

This work is supported by Research Grants Council of Hong Kong (Grant Nos. CUHK2/CRF/08, AoE51911HKU and CUHK4182/09E), the National Science Foundation of China (Grant Nos. 60990314, 60928009, and 61106093), and the Fundamental Research Funds for the Central Universities of China (Grant No. 21611350).

REFERENCES

(1) Qiu, X. H.; Nazin, G. V.; Ho, W. *Phys. Rev. Lett.* **2004**, *92* (20), 206102.
(2) Wu, S. W.; Nazin, G. V.; Chen, X.; Qiu, X. H.; Ho, W. *Phys. Rev. Lett.* **2004**, *93* (23), 236802.
(3) Gao, J.; Xu, J. B.; Zhu, M.; Ke, N.; Ma, D. G. *J. Phys. D: Appl. Phys.* **2007**, *40* (18), 5666−5669.
(4) Horowitz, G.; Hajlaoui, M. E. *Adv. Mater.* **2000**, *12* (14), 1046−1050.
(5) Ostroverkhova, O.; Cooke, D. G.; Hegmann, F. A.; Anthony, J. E.; Podzorov, V.; Gershenson, M. E.; Jurchescu, O. D.; Palstra, T. T. M. *Appl. Phys. Lett.* **2006**, *88* (16), 162101.
(6) Sakanoue, T.; Sirringhaus, H. *Nat. Mater.* **2010**, *9*, 736−740.
(7) Yuen, J. D.; Menon, R.; Coates, N. E.; Namdas, E. B.; Cho, S.; Hannahs, S. T.; Moses, D.; Heeger, A. J. *Nat. Mater.* **2009**, *8*, 572−575.
(8) Troisi, A. *Chem. Soc. Rev.* **2011**, *40*, 2347−2358.
(9) Fratini, S.; Ciuchi, S. *Phys. Rev. Lett.* **2009**, *103* (26), 266601.
(10) Li, L. Q.; Tang, Q. X.; Li, H. X.; Yang, X. D.; Hu, W. P.; Song, Y. B.; Shuai, Z. G.; Xu, W.; Liu, Y. Q.; Zhu, D. B. *Adv. Mater.* **2007**, *19* (18), 2613−2617.
(11) Díez-Pérez, I.; Hihath, J.; Lee, Y. G.; Yu, L. P.; Adamska, L.; Kozhushner, M. A.; Oleynik, I. I.; Tao, N. J. *Nat. Chem.* **2009**, *1*, 635−641.
(12) Pan, S.; Fu, Q.; Huang, T.; Zhao, A. D.; Wang, B.; Luo, Y.; Yang, J. L.; Hou, J. G. *Proc. Natl. Acad. Sci. U.S.A.* **2009**, *106* (36), 15259−15263.
(13) Lu, X.; Hipps, K. W.; Wang, X. D.; Mazur, U. *J. Am. Chem. Soc.* **1996**, *118* (30), 7197−7202.
(14) Lu, X.; Hipps, K. W. *J. Phys. Chem. B* **1997**, *101* (27), 5391−5396.
(15) Gopakumar, T. G.; Meiss, J.; Pouladsaz, D.; Hietschold, M. *J. Phys. Chem. C* **2008**, *112* (7), 2529−2537.
(16) Gopakumar, T. G.; Müller, F.; Hietschold, M. *J. Phys. Chem. B* **2006**, *110* (12), 6060−6065.
(17) Toader, M; Hietschold, M. *J. Phys. Chem. C* **2011**, *115* (7), 3099−3105.
(18) Choi, S. H.; Kim, B. S.; Frisbie, C. D. *Science* **2008**, *320*, 1482−1486.
(19) Choi, S. H.; Risko, C.; Delgado, M. C. R.; Kim, B. S.; Brédas, J. L.; Frisbie, C. D. *J. Am. Chem. Soc.* **2010**, *132* (12), 4358−4368.
(20) Wang, G.; Kim, T. W.; Jo, G.; Lee, T. *J. Am. Chem. Soc.* **2009**, *131* (16), 5980−5985.
(21) Ruppel, L.; Birkner, A.; Witte, G.; Busse, C.; Lindner, Th.; Paasch, G.; Wöll, Ch. *J. Appl. Phys.* **2007**, *102* (3), 033708.
(22) Xie, W. G.; Xu, J. B.; An, J.; Xue, K. *J. Phys. Chem. C* **2010**, *114*, 19044−19047.
(23) Fukagawa, H.; Yamane, H.; Kere, S.; Okudaira, K. K.; Ueno, N. *J. Electron Spectrosc. Relat. Phenom.* **2005**, *144−147*, 475−477.
(24) Barlow, D. E.; Hipps, K. W. *J. Phys. Chem. B* **2000**, *104* (25), 5993−6000.
(25) Metzger, R. M. *Acc. Chem. Res.* **1999**, *32* (11), 950−957.
(26) Janes, D. *Nat. Chem.* **2009**, *1*, 601−603.
(27) Lee, M. J. G. *Phys. Rev. Lett.* **1973**, *30*, 1193−1196.
(28) Kemerink, M.; Alvarado, S. F.; Müller, P.; Koenraad, P. M.; Salemink, H. W. M.; Wolter, J. H.; Janssen, R. A. J. *Phys. Rev. B* **2004**, *70* (4), 045202.

(29) Datta, S.; Tian, W. D.; Hong, S. H.; Reifenberger, R.; Henderson, J. I.; Kubiak, C. P. *Phys. Rev. Lett.* **1997**, *79* (13), 2530−2533.
(30) Fukagawa, H.; Yamane, H.; Kera, S.; Okudaira, K. K.; Ueno, N. *Phys. Rev. B* **2006**, *73* (4), 041302(R).